Inorganic Chemistry
Article

Inorg. Chem. **2010**, *49*, 2911–2919 **2911**
DOI: 10.1021/ic9024662

The Crucial Role of Dispersion in the Cohesion of Nonbridged Binuclear Os → Cr and Os → W Adducts

Stefan Grimme*,† and Jean-Pierre Djukic*,‡

†*Organisch-Chemisches Institut, Westfälische Wilhelms Universität, Corrensstrasse 40, D-48149 Münster, Germany, and* ‡*Institut de Chimie, UMR 7177 CNRS, Université de Strasbourg, 4 rue Blaise Pascal, F-67000 Strasbourg, France*

Received December 12, 2009

The concept of a dative metal−metal bond is generally used to designate the donor−acceptor (DA) interaction of an electron-saturated metal center with another electron-deficient—or unsaturated—metal center. This type of DA bonding extended to the field of coordination complexes constitutes a borderline case of weak metal−metal interaction, among which the so-called metallophilic interactions occurring with 4d, 5d, and other late-transition-metal complexes are the most documented and representative examples. From a general standpoint, the peculiar position of the so-called dative metal−metal bond in chemical bonding stems from its presumed covalent character, which contrasts with the situation encountered with metallophilic interactions, which are essentially supported by dispersion and electrostatic forces and somewhat sustained by relativistic effects. In this study, the nature of the metal−metal bond in nonbridged 5d−3d Os−Cr and 5d−5d Os−W adducts, i.e., $(Me_3P)(CO)_4Os-M(CO)_5$ (M = Cr, W) and $(CO)_5Os-Cr(CO)_5$, was addressed by resorting to state-of-the-art quantum-chemical methods. Semilocal density functional theory (DFT) approximations like Becke−Perdew or TPSS, the double-hybrid B2PLYP functional, as well as the corresponding dispersion, including TPSS-D and B2PLYP-D functionals and the wave-function-based spin-component-scaled second-order perturbative Møller−Plesset theory (SCS-MP2), were used. Energy decomposition analysis combined with the analysis of pairwise interfragment correlation energies from Pipek−Mezey localized molecular orbitals in combination with SCS-MP2 led to a clear demonstration of the significant role of dispersion (London) forces in the stabilization of the title adducts, wherein the Os−metal DA bond bears a rather low covalent character. These results plead in favor of a systematic recourse to dispersion including DFT approximations when addressing organometallic and coordination complexes.

Introduction

Noncovalent interactions are ubiquitous in nature, and their accurate description remains a difficult task.[1−5] van der Waals interactions, $\pi-\pi$ and CH$-\pi$ interactions, and hydrogen bonding contribute greatly to the stereospecificity of chemical processes.[6,7] They can be also used in the rational design of coordination polymers and supramolecular assemblies.[8−13] Because an accurate treatment of these interactions greatly improves the quality of any theoretical investigation of a chemical system or process, great effort is lent to the development of new computational methods capable of providing a pertinent reproduction of experimental observations at relatively moderate computational cost.[14−18] Pykkö's concept of *metallophilic attraction*,[19] which

*To whom correspondence should be addressed. E-mail: grimmes@uni-muenster.de (S.G.), djukic@unistra.fr (J.P.D.). Phone: +49 251 83 36512 (S.G.), +33 03 68 85 15 23 (J.P.D.).

(1) Müller-Dethlefs, K.; Hobza, P. *Chem. Rev.* **2000**, *100*, 143–167.
(2) Kubar, T.; Hanus, M.; Ryjacek, F.; Hobza, P. *Chemistry* **2005**, *12*, 280–290.
(3) Williams, D. H.; Westwell, M. S. *Chem. Soc. Rev.* **1998**, *27*, 57–64.
(4) Britz, D. A.; Khlobystov, A. N. *Chem. Soc. Rev.* **2006**, *35*, 637–659.
(5) Cockroft, S. L.; Hunter, C. A. *Chem. Soc. Rev.* **2007**, *36*, 172–188.
(6) Schuster, O.; Monkowius, U.; Schmidbaur, H.; Ray, R. S.; Krueger, S.; Roesch, N. *Organometallics* **2006**, *25*, 1004–1011.
(7) Ward, T. R.; Collot, J.; Gradinaru, J.; Loosli, A.; Skander, M.; Letondor, C.; Joseph, E.; Klein, G. *Chimia* **2003**, *57*, 586–588.
(8) Doerrer, L. H. *Comments Inorg. Chem.* **2008**, *29*, 93–127.
(9) Borovik, A. S. *Comments Inorg. Chem.* **2002**, *23*, 45–78.
(10) Cooke, G.; Rotello, V. M. *Chem. Soc. Rev.* **2002**, *31*, 275–286.
(11) Turner, D. R.; Pastor, A.; Alajarin, M.; Steed, J. W. *Struct. Bonding (Berlin)* **2004**, *108*, 97–168.
(12) Hunter, C. A. *Chem. Soc. Rev.* **1994**, *23*, 101–109.
(13) Klosterman, J. K.; Yamauchi, Y.; Fujita, M. *Chem. Soc. Rev.* **2009**, *38*, 1714–1725.
(14) Tsipis, A. C.; Orpen, A. G.; Harvey, J. N. *Dalton Trans.* **2005**, 2849–2858.
(15) Zhao, Y.; Truhlar, D. G. *Org. Lett.* **2007**, *9*, 1967–1970.
(16) Minenkov, Y.; Occhipinti, G.; Jensen, V. R. *J. Phys. Chem. A* **2009**, *113*, 11833–11844.
(17) Grimme, S.; Antony, J.; Schwabe, T.; Mück-Lichtenfeld, C. *Org. Biomol. Chem.* **2007**, *5*, 741–758.
(18) Gräfenstein, J.; Cremer, D. *J. Chem. Phys.* **2009**, *130*, 124105.
(19) Pyykkö, P.; Li, J.; Runeberg, N. *Chem. Phys. Lett.* **1994**, *218*, 133–138.

Published on Web 02/05/2010

designates attractive interactions[20−26] between closed-shell 4d, 5d, and late-transition-metal centers,[23,27−32] is considered to result from a combination of effects, among which dispersion forces[33] intervening between the metal centers[34−39] and the ligand retinue of the latter can be central and sustained to some extent by relativistic effects.[40] Recent studies[41,42] have provided more indication on the involvement of dispersion forces in 3d transition-metal complexes containing weak intramolecular intermetallic interactions. From this standpoint, the so-called "dative metal−metal bonds" are borderline cases because in this concept the metal−metal donor−acceptor (DA) interaction entails a significant amount of covalent character.[43] Several such cases, where a dative bond between an electron-deficient metal and a saturated metal was postulated, have been reported in the literature for quite a number of bridged binuclear species,[44−47] with few thorough investigations of the metal−metal interaction though.[48] Pomeroy et al. reported the synthesis and characterization of a series of archetypes of metal−metal DA Lewis adducts presenting the originality of having a nonbridged metal−metal dative bond.[49−51] A variety of examples were further put forward that proved the experimental validity of the concept of dative bonds between different closed-shell metal centers.[27,50,52−58] The synthesis of **3a**−**3c**,[59] for instance, consisted of opposing 18-electron group VIII complexes such as **1a** and **1b** to a range of electron-unsaturated species, such as **2a** and **2b**, possessing a vacant or readily available coordination site (eq 1). This methodology was particularly successful with osmium(0) complexes such as **1a**, because quasi-square-pyramidal carbonylosmium pentacoordinates are rather configurationally stable,[60] a feature that greatly favored, in principle, the direct metal-to-metal interaction and the formation of adducts. Furthermore, it was demonstrated that the photolytical cleavage of **3b**[61,62] was heterolytic in nature, leading to the disruption of the adduct into **1a** and a stabilized form of **2b**, i.e., $LW(CO)_5$ (L = phosphane). In the present Article, the bonding relationship existing in Os−Cr and Os−W complexes such as **3a** and **3b**[59] is investigated by resorting to recently developed DFT-D and wavefunction-based methods. This work complements Nakatsuji et al.'s early investigations[63] of models of **3a**−**3c** and provides conspicuous evidence on the crucial role of dispersion forces in the stabilization of nonbridged so-called dative metal−metal bonds.

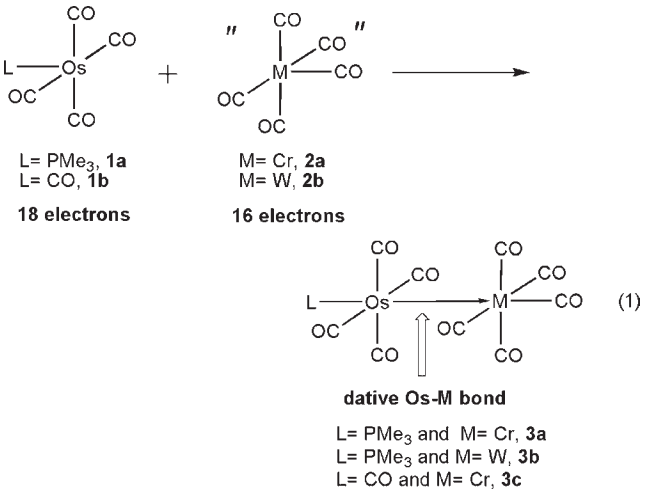

Theoretical and Computational Details

General Procedures. Geometry optimization and singlet ground-state electronic structure determination were performed

(20) Schmidbaur, H. *Gold Bull.* **2000**, *33*, 3–10.
(21) Carvajal, M. A.; Alvarez, S.; Novoa, J. J. *Chem.—Eur. J.* **2004**, *10*, 2117–2132.
(22) Patel, U.; Singh, H. B.; Wolmerhaeuser, G. *Angew. Chem., Int. Ed.* **2005**, *44*, 1715–1717.
(23) Che, C.-M.; Lai, S.-W. *Coord. Chem. Rev.* **2005**, *249*, 1296–1309.
(24) Fernandez, E. J.; Laguna, A.; Lopez-de-Luzuriaga, J. M.; Monge, M.; Olmos, M. E.; Puelles, R. C. *J. Phys. Chem. B* **2005**, *109*, 20652–20656.
(25) Pyykkö, P.; Mendizabal, F. *Inorg. Chem.* **1998**, *37*, 3018–3025.
(26) Crespo, O.; Laguna, A.; Fernandez, E. J.; Lopez-de-Luzuriaga, J. M.; Jones, P. G.; Teichert, M.; Monge, M.; Pyykkö, P.; Runeberg, N.; Schuetz, M.; Werner, H.-J. *Inorg. Chem.* **2000**, *39*, 4786–4792.
(27) Poblet, J. M.; Bénard, M. *Chem. Commun.* **1998**, 1179–1180.
(28) Hermann, H. L.; Boche, G.; Schwerdtfeger, P. *Chem.—Eur. J.* **2001**, *7*, 5333–5342.
(29) Xia, B.-H.; Zhang, H.-X.; Jiao, Y.-Q.; Pan, Q.-J.; Li, Z.-S.; Sun, C.-C. *J. Chem. Phys.* **2004**, *120*, 11487–11492.
(30) Joszai, R.; Beszeda, I.; Benyei, A. C.; Fischer, A.; Kovacs, M.; Maliarik, M.; Nagy, P.; Shchukarev, A.; Toth, I. *Inorg. Chem.* **2005**, *44*, 9643–9651.
(31) Goodwin, A. L.; Keen, D. A.; Tucker, M. G.; Dove, M. T.; Peters, L.; Evans, J. S. O. *J. Am. Chem. Soc.* **2008**, *130*, 9660–9661.
(32) Assadollahzadeh, B.; Schwerdtfeger, P. *Chem. Phys. Lett.* **2008**, *462*, 222–228.
(33) Wang, S.-G.; Schwarz, W. H. E. *J. Am. Chem. Soc.* **2004**, *126*, 1266–1276.
(34) Ford, P. C.; Vogler, A. *Acc. Chem. Res.* **1993**, *26*, 220–226.
(35) Vlcek, A. *Chemtracts* **1998**, *11*, 359–365.
(36) Coppens, P.; Novozhilova, I. V. *Int. J. Quantum Chem.* **2005**, *101*, 611–623.
(37) Chen, Z.-N.; Zhao, N.; Fan, Y.; Ni, J. *Coord. Chem. Rev.* **2009**, *253*, 1–20.
(38) Bardaji, M.; Laguna, A. *Eur. J. Inorg. Chem.* **2003**, 3069–3079.
(39) Jansen, M. *Angew. Chem.* **1987**, *99*, 1136–1149.
(40) Pyykkö, P. *Chem. Rev.* **1997**, *97*, 597–636.
(41) Schwabe, T.; Grimme, S.; Djukic, J.-P. *J. Am. Chem. Soc.* **2009**, *131*, 14156–14157.
(42) Hyla-Kryspin, I.; Grimme, S.; Djukic, J. P. *Organometallics* **2009**, *28*, 1001–1013.
(43) Arndt, L. W.; Darensbourg, M. Y.; Delord, T.; Trzcinska-Bancroft, B. *J. Am. Chem. Soc.* **1986**, *108*, 2617–2627.
(44) Hock, A. A.; Mills, O. S. *Acta Crystallogr.* **1961**, *14*, 139–148.
(45) Edelman, F.; Töfke, S.; Behrens, U. *J. Organomet. Chem.* **1986**, *308*, 27–34.
(46) Kalinin, V. N.; Cherepanov, I. A.; Moiseev, S. K.; Batsanov, A. S.; Struchkov, Y. T. *Mendeleev Commun.* **1991**, 77–78.
(47) Bonifaci, C.; Ceccon, A.; Gambaro, A.; Ganis, P.; Santi, S.; Valle, G.; Venzo, A. *Organometallics* **1993**, *12*, 4211–4214.
(48) Barr, R. D.; Green, M.; Marsden, K.; Stone, F. G. A.; Woodward, P. *J. Chem. Soc., Dalton Trans.* **1983**, 507–512.
(49) Einstein, F. W. B.; Jones, T.; Pomeroy, R. K.; Rushman, P. *J. Am. Chem. Soc.* **1984**, *106*, 2707–2708.
(50) Einstein, F. W. B.; Pomeroy, R. K.; Rushman, P.; Willis, A. C. *Organometallics* **1985**, *4*, 250–255.
(51) Fleming, M. M.; Pomeroy, R. K.; Rushman, P. *J. Organomet. Chem.* **1984**, *273*, C33–C38.
(52) Batchelor, R. J.; Davis, H. B.; Einstein, F. W. B.; Pomeroy, R. K. *J. Am. Chem. Soc.* **1990**, *112*, 2036–2037.
(53) Einstein, F. W. B.; Martin, L. R.; Pomeroy, R. K.; Rushman, P. *J. Chem. Soc., Chem. Commun.* **1985**, 345–346.
(54) Einstein, F. W. B.; Jennings, M. C.; Krentz, R.; Pomeroy, R. K.; Rushman, P.; Willis, A. C. *Inorg. Chem.* **1987**, *26*, 1341–1344.
(55) Shipley, J. A.; Batchelor, R. J.; Einstein, F. W. B.; Pomeroy, R. K. *Organometallics* **1991**, *10*, 3620–3629.
(56) Jiang, F.; Male, J. L.; Biradha, K.; Leong, W. K.; Pomeroy, R. K.; Zaworotko, M. J. *Organometallics* **1998**, *17*, 5810–5819.
(57) Jiang, F.; Biradha, K.; Leong, W. K.; Pomeroy, R. K.; Zaworotko, M. J. *Can. J. Chem.* **1999**, *77*, 1327–1335.
(58) Jiang, F.; Jenkins, H. A.; Biradha, K.; Davis, H. B.; Pomeroy, R. K.; Zaworotko, M. J. *Organometallics* **2000**, *19*, 5049–5062.
(59) Davis, H. B.; Einstein, F. W. B.; Glavina, P. G.; Jones, T.; Pomeroy, R. K.; Rushman, P. *Organometallics* **1989**, *8*, 1030–1039.
(60) Martin, L. R.; Einstein, F. W. B.; Pomeroy, R. K. *Inorg. Chem.* **1985**, *24*, 2777–2785.
(61) Male, J. L.; Davis, H. B.; Pomeroy, R. K.; Tyler, D. R. *J. Am. Chem. Soc.* **1994**, *116*, 9353–9354.
(62) Male, J. L.; Pomeroy, R. K.; Tyler, D. R. *Organometallics* **1997**, *16*, 3431–3438.
(63) Nakatsuji, H.; Hada, M.; Kawashima, A. *Inorg. Chem.* **1992**, *31*, 1740–1744.

by using the methods of the density functional theory (DFT). Starting geometries were extracted from the Cambridge Structural Database, where compounds **3a** and **3b** are referenced under the respective "refcodes" KAMDOR and CEXYIN. The structure of **3c** was built from that of the optimized **3a** by replacing the PMe_3 ligand by CO. The Becke[64]−Perdew[65,66] generalized gradient approximation (GGA) functional implemented in the Amsterdam density functional (ADF)[67,68] package was used throughout the preliminary phase of our investigation (*ADF2008.01*[69]). As opposed to a similar functional that is typically termed BP86, the implementation in ADF employs the Vosko−Wilk−Nusair parametrization[70] for the local-density approximation correlation energy part. In these calculations, scalar relativistic effects were treated within the zeroth-order regular approximation[71,72] (ZORA). As a consequence, in all cases ad hoc all-electron TZP(ZORA) basis sets were used: electronic configurations of atoms were described by a triple-ζ Slater-type orbital (STO) basis set for H 1s, C 2s and 2p, O 2s and 2p, and P 3s and 3p augmented with a 3d single-ζ polarization for O, C, and P atoms.[73] An all-electron STO basis set (TZP) was used for Os and W in which the core electrons are described with double-ζ functions and valence 4f5d and 6s orbitals with triple-ζ functions augmented with a 6p single-ζ polarization function. An adequate polarized triple-ζ (TZP STO) basis set was also used for Cr.[73] Geometry optimizations by energy-gradient minimization were carried out in all cases without symmetry constraint: an integration grid comprised between 4.5 and 6, with an energy-gradient convergence criterion of 10^{-3} au and tight self-consistent-field (SCF) convergence criteria being used. Fragment analysis as well as calculations of vibrational modes (analytical second-derivative[74,75] frequencies) was performed with optimized geometries using ADF subroutines. Vibrational modes were computed in all cases in order to verify that the optimized geometries were related to energy minima. Wiberg bond indexes (WBI) for ADF-optimized geometries were computed with the *GENNBO 5.0* extension of ADF.[76] Representations of molecular structures and orbitals were drawn using *ADFview* v08. The linear transit procedure implemented in *ADF2008* was used to study the gas-phase conformational behavior of compounds **3a**−**3c** and to compute stationary geometries at constrained intermetallic bond lengths. Each structure was fully optimized without symmetry constraint on the remaining parts of the molecule, with the same convergence criteria as that described above. In the conformational study, the dihedral angle ψ (Scheme 1) was varied (1) for **3c**, from its ψ_0 value in the energy-minimum geometry to its $-\psi_0$ value in about 15 steps and (2) for **3a** and **3b**, from its ψ_0 value to a slightly negative value in sufficient steps so as to obtain acceptably precise potentials. In the latter case, no positional constraint was applied on the PMe_3 group, which was allowed to move freely. All geometries obtained by varying the M−M′ bond length were computed so as to meet full convergence with the criteria described above; no constraint was applied to the dihedral angle ψ. The resulting geometries were used subsequently in single-point calculations carried out with the *TURBOMOLE* package at various levels of theory. The corresponding atomic coordinates are provided in the Supporting Information. Single-point calculations employing these geometries were performed with the double-hybrid functional B2PLYP[77] and the meta-GGA functional TPSS[78] together with the standard DFT-D correction.[79] As a wave-function-based technique, we applied spin-component-scaled second-order Møller−Plesset perturbation theory (SCS-MP2),[80] which has proven fair accuracy also for transition-metal complexes. For Os and W atoms, the hitherto unpublished C_6 coefficients [C_6(Os,W) = 81.24 J mol^{-1} nm^{-6}] and van der Waals radii [R_0(Os,W) = 177.2 pm] have been used in the DFT-D correction. These values have been derived from Hartree−Fock (HF) and time-dependent DFT calculations as described previously.[79] All of these computations have been carried out with a slightly modified version of *TURBOMOLE 5.9*.[81] For the heavier atoms, the def2-TZVPP Gaussian basis sets[82] deprived of the f functions on C, O, and P atoms have been used, while for the H atom, the TZVP basis set[83] has been used. For Os and W atoms, effective (small) core potentials[84] for the 60 inner-shell electrons were applied. For the potential curve of **3a**, we have checked basis set convergence by a comparison with the results from a very large and almost complete def2-QZVP[82] basis set. At the TPSS-D level, the curves are essentially parallel and the one with def2-QZVP is merely shifted upward by less than 1 kcal mol^{-1} (which is about 2% of D_e). For all SCF and perturbation correction calculations, we exploited density fitting approaches

Scheme 1. Definition of Dihedral Angle ψ

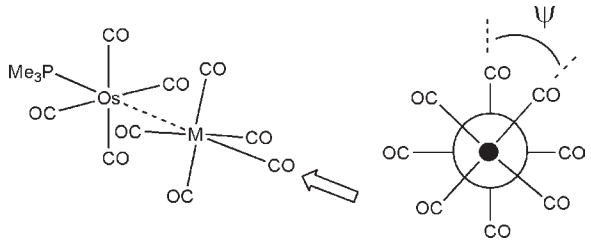

(64) Becke, A. D. *Phys. Rev. A* **1988**, *38*, 3098–3100.
(65) Perdew, J. P. *Phys. Rev. B* **1986**, *34*, 7406.
(66) Perdew, J. P. *Phys. Rev. B* **1986**, *33*, 8822–8824.
(67) te Velde, G.; Bickelhaupt, F. M.; van Gisbergen, S. J. A.; Fonseca-Guerra, C.; Baerends, E. J.; Snijders, J. G.; Ziegler, T. *J. Comput. Chem.* **2001**, *22*, 931–967.
(68) *ADF2003.01, Amsterdam Density Functional*; Department of Theoretical Chemistry, Vrije Universiteit: Amsterdam, The Netherlands, **2003**.
(69) Baerends, E. J.; Autschbach, J.; Bérces, A.; Bickelhaupt, F. M.; Bo, C.; Boerrigter, P. M.; Cavallo, L.; Chong, D. P.; Deng, L.; Dickson, R. M.; Ellis, D. E.; van Faassen, M.; Fan, L.; Fischer, T. H.; Guerra, C. F.; van Gisbergen, S. J. A.; Götz, A. W.; Groeneveld, J. A.; Gritsenko, O. V.; Grüning, M.; Harris, F. E.; van den Hoek, P.; Jacob, C. R.; Jacobsen, H.; Jensen, L.; van Kessel, G.; Kootstra, F.; Krykunov, M. V.; van Lenthe, E.; McCormack, D. A.; Michalak, A.; Neugebauer, J.; Nicu, V. P.; Osinga, V. P.; Patchkovskii, S.; Philipsen, P. H. T.; Post, D.; Pye, C. C.; Ravenek, W.; Rodríguez, J. I.; Ros, P.; Schipper, P. R. T.; Schreckenbach, G.; Snijders, J. G.; Solà, M.; Swart, M.; Swerhone, D.; te Velde, G.; Vernooijs, P.; Versluis, L.; Visscher, L.; Visser, O.; Wang, F.; Wesolowski, T. A.; van Wezenbeek, E. M.; Wiesenekker, G.; Wolff, S. K.; Woo, T. K.; Yakovlev, A. L.; Ziegler, T. *ADF2008.01, Amsterdam Density Functional*; Department of Theoretical Chemistry, Vrije Universiteit: Amsterdam, The Netherlands, **2008**.
(70) Vosko, S. D.; Wilk, L.; Nusair, M. *Can. J. Chem.* **1990**, *58*, 1200–1211.
(71) van Lenthe, E.; Ehlers, A. E.; Baerends, E. J. *J. Chem. Phys.* **1999**, *110*, 8943–8953.
(72) van Lenthe, E.; Baerends, E. J.; Snijders, J. G. *J. Chem. Phys.* **1993**, *99*, 4597–4610.
(73) van Lenthe, E.; Baerends, E. J. *J. Comput. Chem.* **2003**, *24*, 1142–1156.
(74) Bercès, A.; Dickson, R. M.; Fan, L.; Jacobsen, H.; Swerhone, D.; Ziegler, T. *Comput. Phys. Commun.* **1997**, *100*, 247–262.
(75) Wolff, S. K. *Int. J. Quantum Chem.* **2005**, *104*, 645–659.
(76) Glendening, E. D.; Badenhoop, J. K.; Reed, A. E.; Carpenter, J. E.; Bohmann, J. A.; Morales, C. M.; Weinhold, F. *NBO*. 5.0 ed.; Theoretical Chemistry Institute, University of Wisconsin: Madison, WI, **2001**.
(77) Grimme, S. *J. Chem. Phys.* **2006**, *124*, 034108.
(78) Tao, J.; Perdew, J. P.; Staroverov, V. N.; Scuseria, G. E. *Phys. Rev. Lett.* **2003**, *91*, 1464011.
(79) Grimme, S. *J. Comput. Chem.* **2004**, *25*, 1463–1473.
(80) Grimme, S. *J. Chem. Phys.* **2003**, *118*, 9095–9102.
(81) Ahlrichs, R. *TURBOMOLE*, version 5.9; Universität Karlsruhe: Karlsruhe, Germany, **2008**; http://www.turbomole.com.
(82) Weigend, F.; Ahlrichs, R. *Phys. Chem. Chem. Phys.* **2005**, *7*, 3297–3305.
(83) Schäfer, A.; Huber, C.; Ahlrichs, R. *J. Chem. Phys.* **1994**, *100*, 5829–5835.
(84) Andrae, D.; Haeussermann, U.; Dolg, M.; Stoll, H.; Preuss, H. *Theor. Chim. Acta* **1990**, *77*, 123−141. For further details, see: http://www.theochem.unistuttgart.de/pseudopotentials/index.en.html.

(also known as resolution of identity) to speed up the calculations. Respective default auxiliary basis sets[85,86] were taken form the program libraries. For SCS-MP2, the frozen-core approximation was applied (valence orbitals with orbital energies $> -2\ E_h$ were included in the correlation treatment) but not for the SCS-MP2 computations in the localized molecular orbital basis set (SCS-LMP2), in which all electrons haven been correlated. The local transformations were carried out using the Pipek−Mezey scheme,[87] and for the LMP2 computations, a special program written by one of the authors (S.G.) has been used. Note that no excitation amplitudes are discarded in this treatment, and the canonical SCS-MP2 correlation energy is obtained.

Analysis of Pair Correlation Energies. The total correlation energy E_c can be partitioned in an MP2-type (but also in an exact full CI) treatment into pair correlation energies ε_{ij}, i.e.,

$$E_c = \sum_{ij} \varepsilon_{ij} \tag{2}$$

where i and j refer to orbitals i and j, respectively. If the orbitals are spatially localized, they can be grouped together by defining molecular fragments. If orbital i belongs to fragment A and orbital j to fragment B, inter- and intrafragment correlation energies can be defined according to

$$E_c^{\text{intra, A}} = \sum_{ii'} \varepsilon_{ii'} \tag{3}$$

$$E_c^{\text{intra, B}} = \sum_{jj'} \varepsilon_{jj'} \tag{4}$$

$$E_c^{\text{inter, AB}} = \sum_{ij'} \varepsilon_{ij'} \tag{5}$$

where the prime indicates the second electron.

If the orbitals and fragments are similar for different structures (e.g., systems A + B and AB), the correlation energy contribution to the corresponding chemical process $\Delta E_c(\text{A} + \text{B} \rightarrow \text{AB})$ can be partitioned into fragments, e.g., for the interfragment (off-diagonal) part between A and B (that both exist in structures A + B and AB)

$$\Delta E_c^{\text{inter, AB}}(\text{A} + \text{B} \rightarrow \text{AB}) = E_c^{\text{inter, AB}}(\text{AB}) - E_c^{\text{inter, AB}}(\text{A} + \text{B}) \tag{6}$$

While the pair correlation energy sums in eq 3−5 can be very large in magnitude (hundreds of kilocalories per mole), the differences from eq 6 are much smaller and similar to typical chemical energies (a few to a few tens of kilocalories per mole). Note that if A + B and AB correspond to dimers of atoms or molecules at large and small distances, respectively (and A and B correspond to the two monomers), the quantity on the left side of eq 6 equals the "true" dispersion energy (attractive part of the van der Waals potential) in a noncovalent interaction. In our case, A + B and AB are for the complex with short and infinite M−M distances, respectively, and A and B are the two ML_n fragments. We interpret $\Delta E_c^{\text{inter,AB}}$ as an (intra)molecular dispersion energy, although it is clear that the concept of London dispersion (van der Waals attraction) is based on the perturbation theory and thus is only valid for large distances and weak interactions. This view is strongly supported by the results discussed below because the $\Delta E_c^{\text{intra}}$ terms in eqs 3 and 4 (which should be large in absolute magnitude when the electronic structure changes considerably) are essentially zero along our dissociation coordinate. Further numerical evidence for our interpretation in the case of conformational processes in (bio)organic model systems is given in the literature.[88]

Energy Decomposition Analysis (EDA). In order to gain insight not only into the correlation contributions to binding but also for the other electronic interactions, we performed a standard EDA.[89,90] This allows one to partition the interaction energy from a supermolecular DFT-D computation into chemically meaningful parts. EDA has proven to give detailed information about the nature of chemical bonding[91] as well as for interactions in hydrogen-bonded systems,[92] in supramolecular structures,[93] and for transition-metal complexes.[94] The formation of bonding between two fragments is divided into three physically plausible steps. In the first step, the fragment electronic densities (in the frozen geometry of the supermolecule) are superimposed, which yields the quasi-classical electrostatic interaction energy (ES). Renormalization and orthogonalization of the product of monomer wave functions yields a repulsive energy term (often called the Pauli exchange repulsion, EXR). In the final step, the molecular orbitals are allowed to relax to their final form, which yields the (usually stabilizing) induction energy. This term (called OICT) also includes (covalent) orbital interaction and charge-transfer (CT) terms that are dominating for normal covalent bonds. The (damped) dispersion energy term is calculated with the usual DFT-D approach. The total interaction energy is

$$\Delta E = E_{\text{EXR}} + E_{\text{ES}} + E_{\text{OICT}} + E_{\text{DISP}} \tag{7}$$

and it differs from the true interaction energy only by the energy necessary to bring the optimum monomer geometries into the form they have in the supermolecule. This deformation energy is very small in our cases ($< 5\%$ of ΔE) and is not discussed further. We also will discuss the sum of EXR and ES [called the first-order (E_1) interaction energy], which can be interpreted as the semiclassical contribution to binding when the two other quantum mechanical parts (constructive interference of atomic wave functions as well as nonlocal electron correlations) would be absent (i.e., classical but Pauli principle obeying electrons).

Results and Discussion

Electronic Structure. Shortly after Pomeroy's first report on the syntheses of **3a**−**3c**,[59] the group of Nakatsuji et al.[63] published an article addressing the electronic structure and nature of the metal−metal bond in the title compounds. The work resorted to an ab initio approach at the HF level of simplified models of **3a**−**3c**, whereby the trimethylphosphane ligand was replaced by CO and the geometries were not relaxed. The equilibrium value of the Os−M (M = Cr, W) distance R_e in those adducts was

(85) Weigend, F.; Köhn, A.; Hättig, C. *J. Chem. Phys.* **2002**, *116*, 3175–3183.
(86) Eichkorn, K.; Weigend, F.; Treutler, O.; Ahlrichs, R. *Theor. Chem. Acc.* **1997**, *97*, 119–124.
(87) Pipek, J.; Mezey, P. G. *J. Chem. Phys.* **1989**, *90*, 4916–4926.
(88) Grimme, S.; Mück-Lichtenfeld, C.; Antony, J. *Phys. Chem. Chem. Phys.* **2008**, *10*, 3327–3334.
(89) Morokuma, K. *J. Chem. Phys.* **1971**, *55*, 1236–1244.
(90) Kitaura, K.; Morokuma, K. *Int. J. Quantum Chem.* **1976**, *10*, 325–340.
(91) Bickelhaupt, F. M.; Baerends, E. J. *Rev. Comput. Chem.* **2000**, *15*, 1–86.
(92) Swart, M.; Guerra, C. F.; Bickelhaupt, F. M. *J. Am. Chem. Soc.* **2004**, *126*, 16718–16719.
(93) Parac, M.; Etinski, M.; Peric, M.; Grimme, S. *J. Chem. Theory Comput.* **2005**, *1*, 1110–1118.
(94) Frenking, G. In *Encyclopedia of Computational Chemisty*; von Ragué-Schleyer, P., Ed.; John Wiley: New York, 1998; Vol. *5*, p 3073.

Table 1. Computed [Becke−Perdew/TZP(ZORA) Level] and Experimental Geometrical Features for Complexes **3a**−**3c**

	3a (M = Cr)		**3b** (M = W)		**3c** (M = Cr)
	calcd	exptl[a]	calcd	exptl[a]	calcd
Os−M, R_e (pm)	309.8	297.87(14)	317.0	307.56(5)	307.9
M−CO_{eq} (pm)	189.3	190.4(9)	204.6	202.1(7)	189.6
M−CO_{ax} (pm)	183.3	181.9(9)	197.1	196.5(8)	183.7
Os−CO_{eq} (pm)	196.2	195.2(9)	196.2	195.0(8)	197.6
Os−L (pm)	238.4[b]	235.1(2)[b]	238.8[b]	235.9(2)[b]	194.3[c]
M−Os−CO_{eq} (pm)	82.6	81.9	83.2	80.2	81.8
ψ_0 (deg)	44.5	42.8	43.0	45.0	45.6

[a] Compare ref 59. [b] L = PMe_3. [c] L = CO.

essentially deduced from plots of the potential energy versus the intermetallic distance. The resulting R_e values were close to the experimental (R_0) values obtained for **3a** and **3b** by X-ray diffraction analysis. In order to verify Nakatsuji et al.'s assumptions on the electronic structure of compounds **3a**−**3c**, singlet ground-state relaxed geometries of the latter were computed by the energy-gradient-minimization method on the real molecules in the gas phase using the Becke−Perdew/TZP(ZORA) method, which has already proven in previous reports to be adequate for dinuclear carbonyl complexes.[95,96] Table 1 lists the main geometrical parameters of optimized complexes **3a**−**3c**. Most geometric features were well reproduced within a range of 3 pm. The largest discrepancies (overestimations) can be noticed for the Os−Cr distance R_e (ca. 13 pm) in **3a** and for the Os−W distance (ca. 9.5 pm) in **3b**. As discussed below, these errors are attributed to the missing intramolecular London dispersion interactions in this simple (standard) DFT approach. A conformational analysis was also carried out to verify that the antieclipsed conformation observed in the X-ray diffraction structure was related to an absolute minimum of energy. This was carried out by decreasing dihedral angle ψ stepwise (Scheme 1) within the $\psi_0 > 0 > -\psi_0$ range and by allowing each intermediate geometry to relax to full convergence at each constrained ψ angle value. The corresponding barriers-to-rotation for **3a**−**3c** were estimated to be ca. 3.5 kcal mol^{-1}, with syn-eclipsed conformers being associated with a slightly elongated Os−M segment due to the elevated electronic repulsion between the equatorial CO ligands of different fragments when those face each other (cf. the Supporting Information).

Frontier orbital interaction diagrams were computed using ADF's fragment orbital analysis utility, which permits a quantification of the contributing interacting molecular orbitals of the considered fragments, with the latter considered here consisting of the $L(CO)_4Os$ and $M(CO)_5$ moieties in their so-called "prepared" geometries in **3a**−**3c**. Figure 1 displays a simplified interaction diagram that essentially reproduces the trends pointed out by Nakatsuji et al.[63] The so-called dative bond results from a DA interaction between the highest occupied molecular orbital (HOMO) of the $L(CO)_4Os$ fragment and the lowest unoccupied molecular orbital (LUMO) of the $M(CO)_5$ fragment (Figure 1). Completing Nakatsuji et al.'s statements, our analysis shows that the interaction between the two metals is unbalanced. The strongest contribution to the bonding orbital in all three cases **3a**−**3c** is on the HOMO of the Os-centered moiety (77.8% in **3a**, 79.0% in **3b**, and 78.0% in **3c**) and the weakest on the LUMO of the M-centered moiety (19.6% in **3a**, 17.0% in **3b**, and 18.9% in **3c**). The former HOMO orbitals in prepared fragments **1a** and **1b** do not have the σ-type symmetry mentioned by Nakatsuji et al.,[63] and furthermore they are not centered at the Os atom. Analysis indicates a rather significant delocalization of the HOMO over the four equatorial carbonyl ligands and the Os center. A similar picture can be drawn for the delocalized LUMO of $M(CO)_5$ (M = Cr, W). The frontier orbitals considered here both result from a combination of the metal-centered d_z^2 with p_z orbitals at the C and O atoms of the four equatorial CO ligands. WBIs[97] of the intermetallic segment were calculated for all three complexes **3a**−**3c** from the orthogonal natural atomic orbital bases using GENNBO. The values of WBIs are all below or equal to 0.1, which clearly suggests a poor contribution of covalence in the metal−metal interaction.[97] The plot of the Coulombic (electrostatic) potential over the isosurface of the SCF density conspicuously shows (Figure 2) for all three complexes very low accumulation of charge densities around the two metal centers and slight differences in potential between the two vicinal metal centers. This result is in agreement with the EDA discussed below that electrostatic and induction (polarization) terms for the binding process are small.

Dispersion in Adduct 3a. The potential energy curves along the M−M stretching coordinate for **3a** at various levels of theory are shown in Figure 3. Together with results for the dispersion-corrected ("-D" appended) and uncorrected TPSS functional, we discuss for comparison HF and SCS-MP2 wave-function-based data as well as the very accurate B2PLYP-D double-hybrid functional result. According to test calculations, the nonempirical TPSS method yields curves very similar to those of other (meta)-GGA approximations [e.g., the Becke−Perdew/TZP(ZORA) method used above], and therefore we will discuss it as a typical example.

As can be seen clearly in Figure 3, the dispersion correction has a strong impact on the shape of the curves and, in particular, on the depth of the minimum (dissociation energy D_e). The TPSS value of about 24.2 kcal mol^{-1} is almost doubled to 42.1 kcal mol^{-1} at the TPSS-D level. The major part of the difference (termed in the following the "dispersion effect") seems to result from the M−L and M−M interactions, while the L−L contribution is smaller (see below). Keeping in mind that SCS-MP2 typically overbinds transition-metal complexes by 10−20% of D_e[98] and considering that there might be some remaining basis set incompleteness effects for B2PLYP-D, the TPSS-D, B2PLYP-D, and SCS-MP2 curves are in good agreement, suggesting a "true" D_e value of about 40−45 kcal mol^{-1}. It seems very encouraging that two DFT approximations with very different ingredients and constructed very differently provide very similar curves. Note also the almost identical energies of

(95) Barckholtz, T. A.; Bursten, B. E. *J. Organomet. Chem.* **2000**, *596*, 212–220.
(96) Rosa, A.; Ehlers, A. W.; Baerends, E. J.; Snijders, J. G.; te Velde, G. *J. Phys. Chem.* **1996**, *100*, 5690–5696.
(97) Mayer, I. *Theor. Chim. Acta* **1985**, *67*, 315–322.
(98) Hyla-Kryspin, I.; Grimme, S. *Organometallics* **2004**, *23*, 5581–5592.

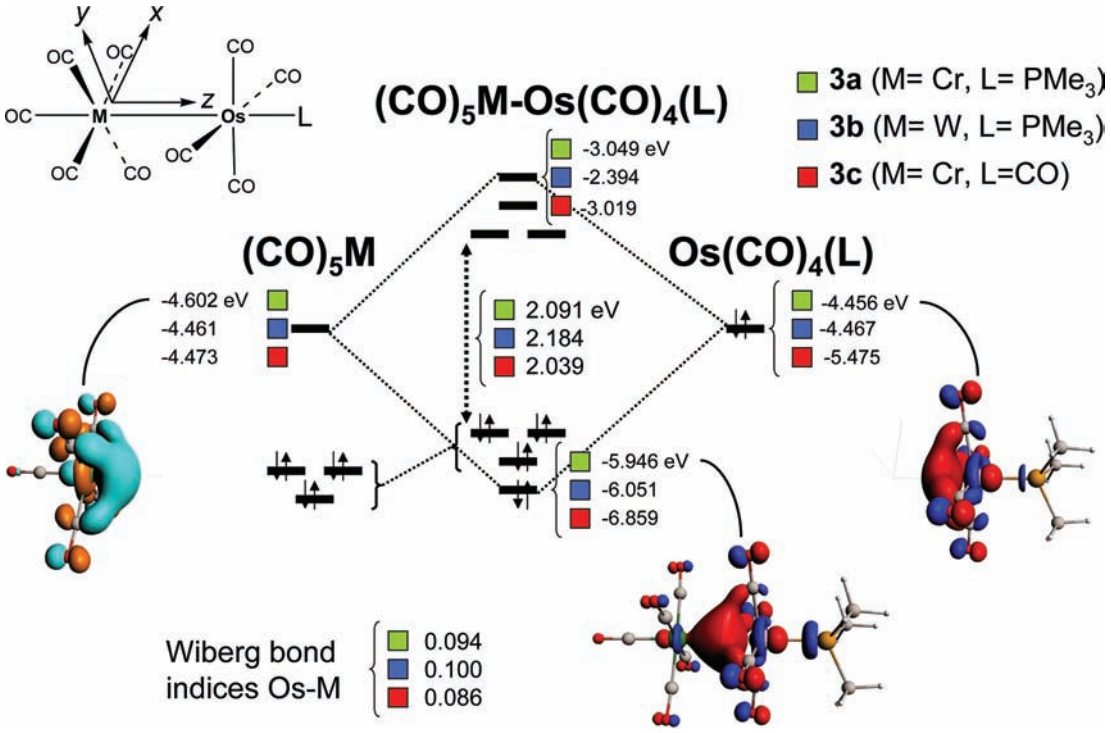

Figure 1. Expanded formula of compounds **3a**−**3c** considered in this study with a simplified fragment orbital interaction diagram [Becke−Perdew/all-electron TZP(ZORA)] and *ADFview2008* drawings of interacting frontier HOMO (red-dark blue) and LUMO (orange-cyan) Kohn−Sham orbitals of prepared fragments **1a** and **2a** and of the resulting HOMO−4 bonding orbital in **3a**. For the sake of clarity, only those orbitals related to **3a** are depicted here with an isosurface contour value of 0.04 e bohr^{-3}.

the three approaches in the asymptotic region (R > 350 pm), which differ significantly from the uncorrected TPSS and HF results. This strongly underlines the conclusion that long-range dispersion-type interactions (at medium interatomic distances) play a crucial role in this system.

The dispersion effect is smaller but still visible for the equilibrium distance between the metals (R_e). Uncorrected TPSS yields a too long bond (by about 6.2 pm), while TPSS-D and B2PLYP-D are too short by 1.2 and 6.8 pm, respectively. SCS-MP2 strongly underestimates the M−M distance by 15.8 pm, which is a typical behavior for this method (which is, however, much better than the standard MP2, the results of which are not shown). Apparently, TPSS-D provides the best result when compared directly with the experimental value of R_e = 298 pm. However, the potential is rather anharmonic, and corrections for this would certainly increase the computed M−M distance, thereby bringing the TPSS-D and B2PLYP-D results into even better agreement with the experimental value. According to our (limited) experience with DFT-D for metallic systems, it seems as if the method provides in its current form slightly too large dispersion corrections, which perfectly fits to the above conclusions.

One of the convenient features of DFT-D is the ease with which the various contributions to binding can be analyzed. In our case, we are interested in a separation of the M−M, M−L, and L−L interfragment dispersion interactions. This can be accomplished by setting the dispersion coefficients of the two metal atoms to zero. The resulting potential curve displayed in Figure 3 thus only contains the dispersion interaction between the ligands. Their contribution is 7.2 kcal mol^{-1} to D_e, which is about a third of the total dispersion correction. This allows the conclusion that the M−M and M−L parts make up the majority of the dispersion effect, but all terms are more or less equally important.

A possible shortcoming of this analysis is that it is based on an atom-pairwise partitioning with fixed dispersion coefficients, a description that is possibly inappropriate for the intramolecular dispersion effects in a bimetallic complex at relatively short interfragment distances. In order to address this point, we have performed for **3a** a localized wave-function-based analysis using the SCS-LMP2 approach. Although SCS-LMP2 (which is for the total interaction identical with SCS-MP2) provides slightly to strongly interacting ML_n fragments, the general picture should be correct at a semiquantitative level. Figure 4 shows the correlation energy contributions to D_e (i.e., the HF energy is omitted) along the dissociation pathway.

These results are very important not only for the understanding of the binding in **3a** but also from the methodological point of view regarding the question of the reliability of DFT-D. First, it is noted that the intrafragment correlation energy is practically constant along the reaction coordinate. This indicates minor changes of the basic electronic structure in the fragments along the dissociation and supports an interpretation of the process as dispersion-driven (interfragment change of correlation energy only). Importantly, the interligand (L−L) contribution from DFT-D and SCS-LMP2 is very similar, and they deviate from each other by more than about 10% only at short distances where in DFT-D the necessary damping function comes into play (for

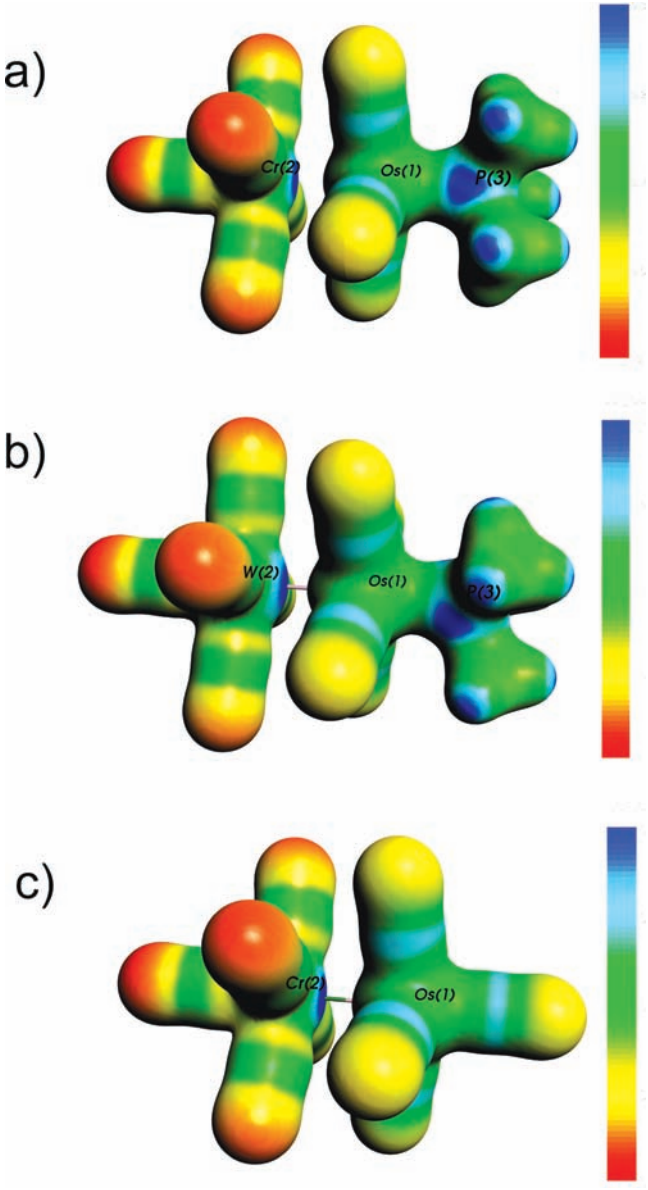

Figure 2. *ADFview2008* plot of the Coulombic potential over the isosurface of the SCF density (contour value 0.035 e bohr^{-3}) for the singlet ground-state structures of **3a**−**3c**: (a) **3a** (red, −0.005 73 au; blue, 0.326 au); (b) **3b** (red, −0.005 94 au; blue, 0.326 au); (c) **3c** (red, 0.0121 au; blue, 0.343 au).

SCS-LMP2, a similar effect results from the strongly repulsive HF contribution [not shown]). Also similar to the DFT-D result discussed above, the M−M and M−L contributions are together about two-thirds of the total correlation energy change. At longer distances, the M−L correlations are stronger, while for shorter M−M distances, the dispersion interactions between the spatially close-lying metal shells become more important. Note, however, that the separation of the ligand and metal parts in the fragment is not so clear-cut because some of the metal-centered localized orbitals (LMO) have significant contributions from the carbonyl groups. On the other hand, no problems have been observed in the assignment of LMOs to the OsL_5 or CrL_5 fragments, respectively. In summary, the SCS-LMP2 analysis strongly supports the DFT-D picture of binding as a dispersion-driven DA interaction.

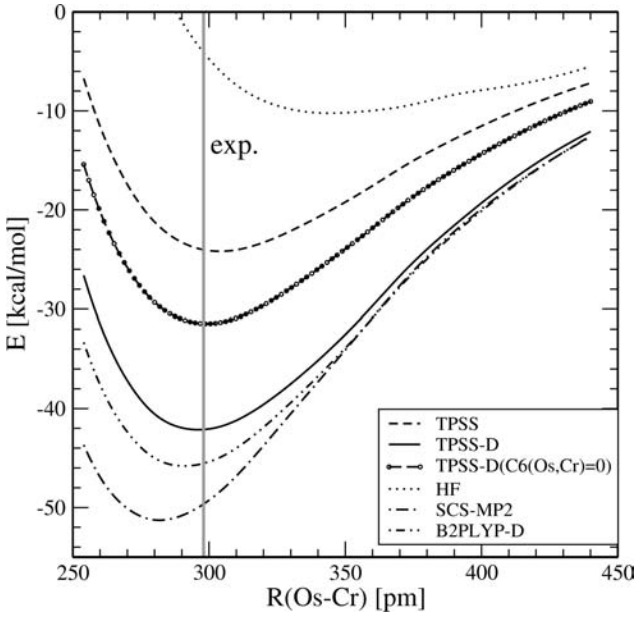

Figure 3. Potential energy curves for **3a** based on single-point ecp-def2-TZVPP computations. The structures for each of the points on the dissociation coordinate have been optimized at the Becke−Perdew/TZP-(ZORA) level. In the curve labeled C_6(Os,Cr) = 0, the dispersion coefficients of the Os and Cr atoms in the DFT-D correction have been set to zero.

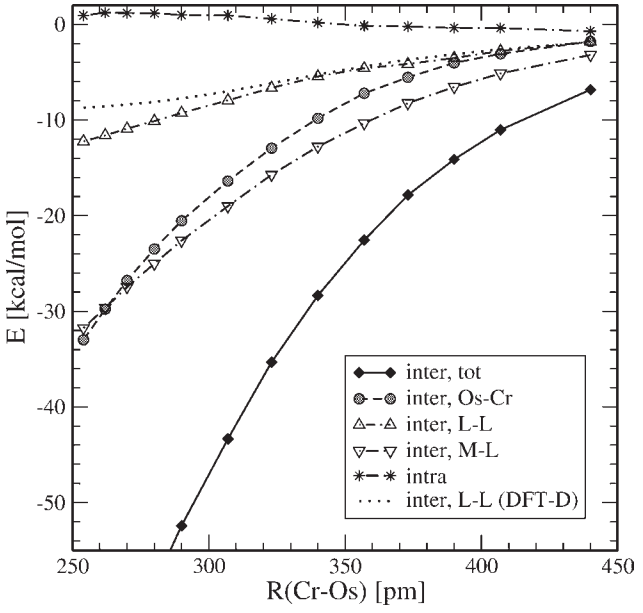

Figure 4. Correlation energy contributions (inter- and intrafragment) to the dissociation energy (i.e., the HF energy is omitted) along the dissociation path for **3a** at the SCS-LMP2/ecp-def2-TZVPP level. For comparison, the interligand DFT-D contribution is also given.

Finally, we want to discuss the question of covalency and the degree of DA character with the help of EDA. The corresponding energy curves of **3a** in comparison to those of Me_3N-BMe_3 are given in Figure 5.

As expected for a DA bond with some covalent character, the attractive ES interaction cannot fully overcompensate for the repulsive Pauli term so that in first-order E_1 (i.e., no orbital, induction, and CT interactions), only a very weak binding for **3a** is found. For the archetypical case of Me_3N-BMe_3, the E_1 potential is

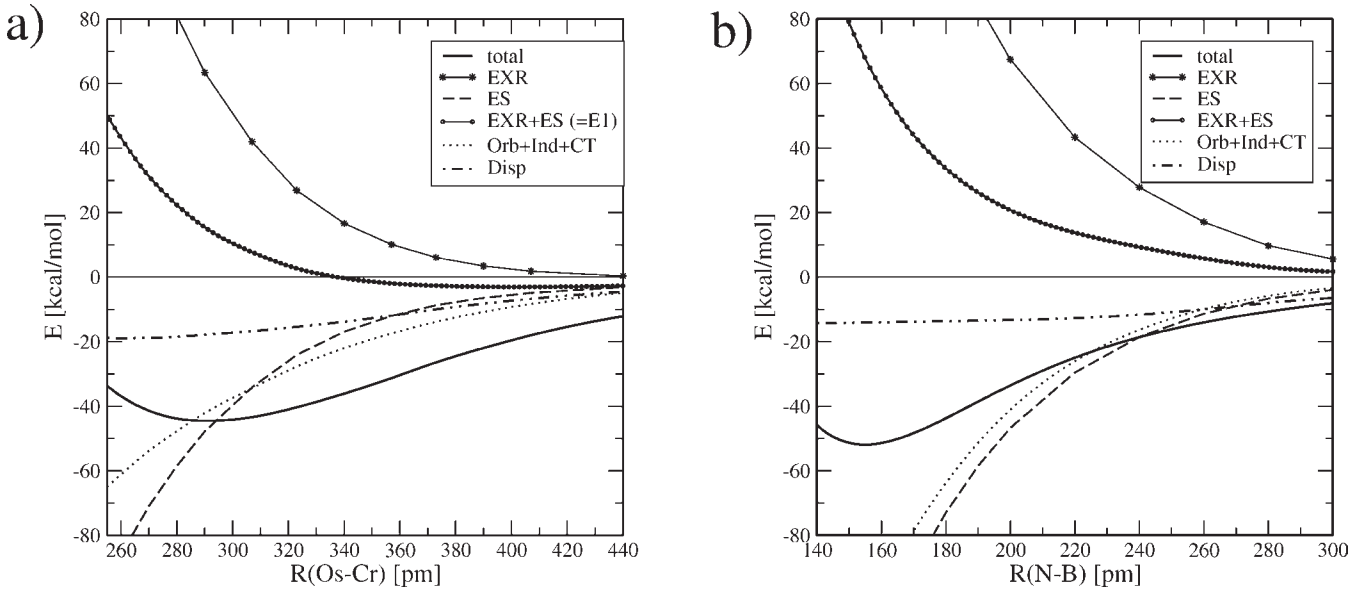

Figure 5. Energy contributions to binding from EDA at the TPSS-D/ecp-def2-TZVPP level of theory: (a) **3a**; (b) Me_3N-BMe_3. The total interaction energy differs slightly from those given in Figure 2 by the fragment relaxation (also called deformation) energy, which is not included here.

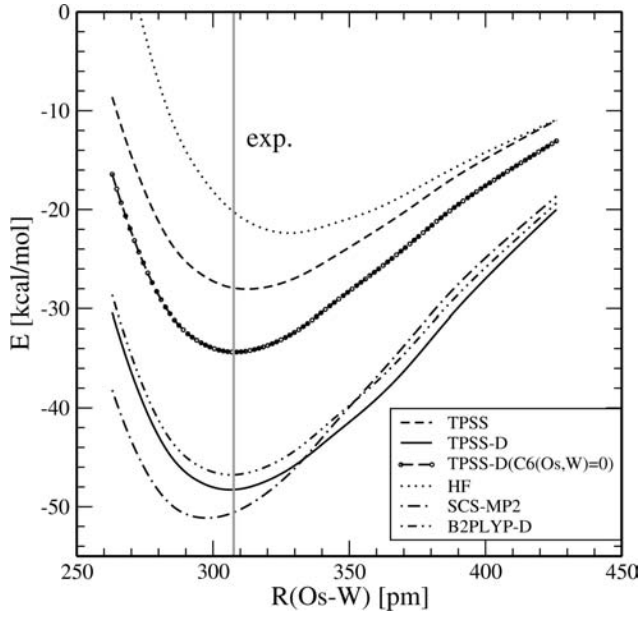

Figure 6. Potential energy curves for **3b** based on single-point ecp-def2-TZVPP computations. The structures for each of the points on the dissociation coordinate have been optimized at the Becke−Perdew/TZP-(ZORA) level. In the curve labeled C_6(Os,W) = 0, the dispersion coefficients of the Os and W atoms in the DFT-D correction have been set to zero.

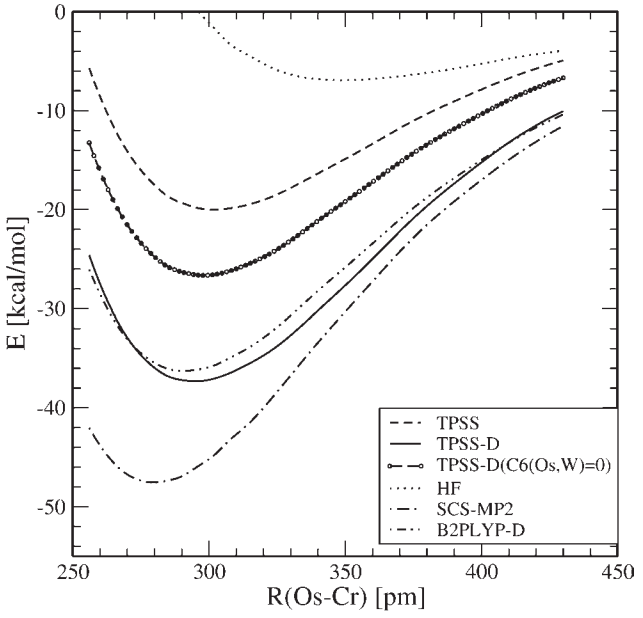

Figure 7. Potential energy curves for **3c** based on single-point ecp-def2-TZVPP computations. The structures for each of the points on the dissociation coordinate have been optimized at the Becke−Perdew/TZP-(ZORA) level. In the curve labeled C_6(Os,Cr) = 0, the dispersion coefficients of the Os and Cr atoms in the DFT-D correction have been set to zero.

more repulsive (although the electrostatic interaction is better than that in **3a**), which indicates a higher covalency. Moreover, the dispersion part is less important. This is different for the metal−metal DA interaction, for which the OICT contribution is *less* than the total interaction energy near equilibrium. Although it is the dominating attractive part, only together with the large dispersion correction, a quantitative description of the M−M binding is observed. Our conclusion that the M−M interaction in **3a** (and this holds for the other systems as well; see below) can be classified as a dispersion-driven DA bond with a small degree of covalency is further supported by Wiberg's covalent bond order,[97] which is computed to be about 0.2 for **3a** near the minimum at this level [and in agreement with the Becke−Perdew/TZP(ZORA) results given above]. The corresponding value for the example of Me_3N-BMe_3 is much larger (about 0.6), which is in line with the larger OICT term.

Adducts 3b and 3c. Analogous computations have been performed for **3b** and **3c**. The corresponding potential energy curves are shown in Figures 6 and 7. Replacing the Cr atom by a W atom in **3b** increases the D_e value slightly to about 48 kcal mol^{-1}. As expected, SCS-MP2 is closer to both DFT-D results (perturbation methods generally

perform better for 4d/5d compared to 3d metal complexes). The main conclusions described above for **3a** also hold for the valence isoelectronic system. Note, however, the larger contribution of dispersion compared to **3a** (21 vs 18 kcal mol^{-1}), which is explained by the larger C_6 coefficient for W compared to that of Cr.

Compared to **3a**, which differs from **3c** by the exchange of a carbonyl with a phosphane group, the D_e values decrease by about 5 kcal mol^{-1}. The TPSS-D and B2PLYP-D methods again yield very similar results, while SCS-MP2 substantially overbinds. The equilibrium distances as well as the dispersion effect (17.3 kcal mol^{-1}) are about the same in both complexes. In summary, we can conclude that both, modification of one of the ligands and exchange of one of the metals, have almost no impact on the predominant interactions between the fragments.

Conclusions

This study has clearly demonstrated that, even for small transition-metal complexes with sterically nondemanding substituents, long-range dispersion-type interactions are of the utmost importance for a quantitative understanding of bonding. These conclusions are based on state-of-the-art quantum-chemical calculations with extended atomic orbital basis sets and appropriate treatment of scalar-relativistic effects. Semilocal DFT approximations (like Becke-Perdew or TPSS), which do not account for the corresponding nonlocal correlation energy terms, underestimate the metal−metal dissociation energy by about 50% (roughly 15−20 kcal mol^{-1}) in our examples. This is important because these methods are applied routinely in many areas of organometallic chemistry. Furthermore, because of often larger ligands or substituents, dispersion-type interactions are expected to be even larger in many "real" compounds, and we thus strongly recommend the application of dispersion-corrected DFT for almost all quantum-chemical "real-life" problems. Although based, in part, on perturbation theory, the fully nonlocal double-hybrid density functional B2PLYP-D has again proven its outstanding accuracy and robustness also for transition-metal complexes. Our wave-function-based analysis (by an LMO partitioning of the correlation energy) leads to the important conclusion that the corresponding energy terms can be computed with reasonable accuracy with the semiclassical and physically sound DFT-D method as an atom-pairwise sum of damped R^{-6} potentials. The necessary atomic parameters seem to be accurate enough even for the here investigated 3d/5d metals, as indicated by a comparison of the TPSS-D, B2PLYP-D (for which the -D correction is only 55% compared to that of TPSS-D), and SCS-MP2 results. The metal−metal interaction in these complexes can be classified as a *dispersion-driven DA bond* with a small covalent contribution. The change of the electronic structure of the fragments in the bond formation is negligible, as indicated by small changes of the intrafragment correlation energy. The picture provided by SCS-LMP2 and DFT-D methods regarding the contribution of M−M, M−L, and L−L dispersion parts to binding is roughly the same; i.e., they all account for about a third of the correlation contribution to the interaction.

Acknowledgment. The authors gratefully acknowledge the Deutsche Forschungsgemeinschaft (in the framework of SFB 858), the Centre National de la Recherche Scientifique, and the Alexander von Humboldt Foundation for their support.

Supporting Information Available: (1) Cartesian coordinates and total bonding energies of optimized singlet ground-state geometries, (2) computed vibrational modes and frequencies, (3) Cartesian coordinates of relaxed geometries obtained in the linear transit investigation of the variation of R_e, and (4) Cartesian coordinates of optimized singlet ground-state geometries of fragments **1a**, **1b**, **2a**, and **2b**. This material is available free of charge via the Internet at http://pubs.acs.org.